

# OmniSplat: Taming Feed-Forward 3D Gaussian Splatting for Omnidirectional Images with Editable Capabilities

Suyoung Lee\*<sup>1</sup> Jaeyoung Chung\*<sup>1</sup> Kihoon Kim<sup>2</sup> Jaeyoo Huh<sup>2</sup>

Gunhee Lee<sup>3</sup> Minsoo Lee<sup>3</sup> Kyoung Mu Lee<sup>1,2</sup>

<sup>1</sup>Dept. of ECE & ASRI, <sup>2</sup>IPAI, Seoul National University, <sup>3</sup>LG AI Research, Seoul, Korea  
{esw0116, robot0321, kihoon96}@snu.ac.kr jaeyoo900@gmail.com  
{gunhee.lee, minsoo.lee}@lgresearch.ai kyoungmu@snu.ac.kr

## Abstract

Feed-forward 3D Gaussian Splatting (3DGS) models have gained significant popularity due to their ability to generate scenes immediately without needing per-scene optimization. Although omnidirectional images are getting more popular since they reduce the computation for image stitching to composite a holistic scene, existing feed-forward models are only designed for perspective images. The unique optical properties of omnidirectional images make it difficult for feature encoders to correctly understand the context of the image, and make the Gaussian non-uniform in space, which hinders the image quality synthesized from novel views. We propose OmniSplat, a pioneering work for fast feed-forward 3DGS generation from a few omnidirectional images. We introduce Yin-Yang grid and decompose images based on it to reduce the domain gap between omnidirectional and perspective images. The Yin-Yang grid can use the existing CNN structure as it is, but its quasi-uniform characteristic allows the decomposed image to be similar to a perspective image, so it can exploit the strong prior knowledge of the learned feed-forward network. OmniSplat demonstrates higher reconstruction accuracy than existing feed-forward networks trained on perspective images. Furthermore, we enhance the segmentation consistency between omnidirectional images by leveraging attention from the encoder of OmniSplat, providing fast and clean 3DGS editing results.

## 1. Introduction

The reconstruction of holistic 3D scenes from multi-view images is one of the fundamental problems in computer vision with emerging applications such as virtual reality (VR), augmented reality (AR), robotics, or autonomous navigation. The goal is to rapidly and accurately create *holistic* 3D representations of environments. Recent advance-

\*indicates equal contribution.

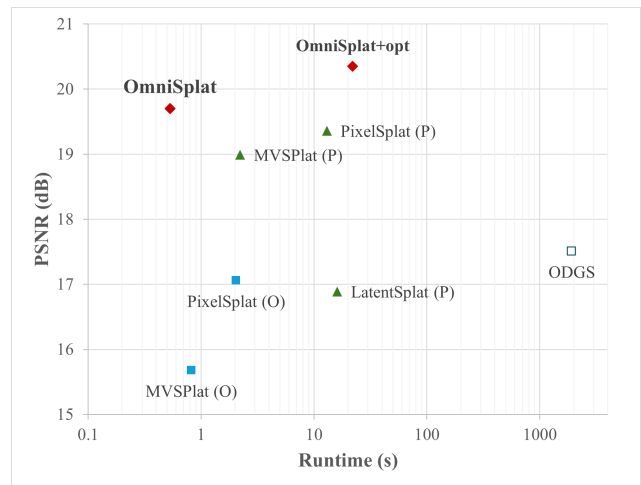


Figure 1. **PSNR-runtime trade-off.** A chart of reconstruction performance-runtime trade-off in novel view image on Ricoh [6]. OmniSplat shows the best trade-off compared to the original feed-forward networks for perspective images and models with optimization designed for omnidirectional images.

ments have focused on feed-forward scene generation networks [2, 4, 29], which are capable of generating 3D Gaussian splatting (3DGS) representations directly from a few input images without scene-wise optimization [18]. These models estimate plausible 3D Gaussian parameters by leveraging priors learned from large-scale datasets and achieve more than 30 times faster than optimization-based methods. However, they often encounter challenges in constructing a holistic scene due to the perspective camera with a limited field of view. Constructing a holistic scene using multiple perspective images in a pair-wise manner incurs significant drawbacks in terms of both computational efficiency and reconstruction quality. Instead, omnidirectional images have become increasingly prevalent due to their ability to capture a wide field of view within a single image. They are computationally efficient as they reduce the amount of data

and computation for image stitching to represent an entire scene compared to perspective images. Despite the advantages, no attempts are made to estimate the parameters of 3D Gaussians directly in the omnidirectional image domain due to insufficient omnidirectional video data for training the Transformer-based network.

Leveraging advanced pre-trained networks to achieve the goal presents some challenges that must be overcome. Standard omnidirectional (or equirectangular) images or fisheye images cannot be directly processed with pre-trained networks, due to their non-uniform structure. For instance, the horizontal length of the object is stretched in polar regions of omnidirectional images, making the shape of the object different from perspective images. Thus, the existing pre-trained network trained with perspective images often miscomprehends the context in the omnidirectional images, extracting unintended features. In addition, such non-uniform grids promote uneven Gaussian generation, which degrades the quality of novel view synthesis. When synthesizing an omnidirectional image from a novel view using non-uniformly distributed Gaussians, the high sampling frequency near the poles results in stripe-like artifacts.

To address these challenges, we propose **OmniSplat**, the first feed-forward 3DGS estimation from a few omnidirectional images. We decompose each omnidirectional image into two images using Yin-Yang grid [17]. The Yin-Yang decomposition is conducted by cutting a sphere into two pieces, similar to the threads of a tennis ball, and arranging them on a plane. Compared to other spherical representation methods such as equirectangular, fish-eye, icosahedral [7] or cubed-sphere [23], the Yin-Yang grid has two advantages: quasi-uniformness and structured grid. First, the quasi-uniformness of the Yin-Yang grid greatly reduces the distortion of omnidirectional images caused by equirectangular projection, making the image much more similar to perspective images. Moreover, Yin-Yang’s structured grid can exploit the strong prior of the existing pre-trained feed-forward networks, whereas the other shapes, like icosahedrons, have a different topology from typical images, making it impossible to utilize the power of existing pre-trained models. After the Gaussians are created in the space, we propose a Yin-Yang rasterizer to render Yin and Yang images for a novel view. Then, the two rasterized images are transformed and combined into the final omnidirectional image in a pixel space. This eliminates many artifacts caused by high sampling frequency in polar regions when using an omnidirectional rasterizer [21].

Extensive experiments validate the effectiveness of our method, showing that it outperforms both the optimization-based omnidirectional 3DGS method (ODGS) and typical feed-forward generation networks in novel-view omnidirectional image reconstruction. As described in Figure 1, OmniSplat shows the fastest synthesis speed while reach-

ing the highest PSNR than any other models. Also, with a small number of optimizations, OmniSplat+*opt* shows overwhelming performance to other networks including ODGS with similar inference time to PixelSplat (P), a feed-forward model with perspective images.

Additionally, we observed that the proposed architecture is well-suited for fast and efficient 3D editing. We utilize the attention scores obtained during the reconstruction process, finding multiview-consistent semantic segmentation. Using this matched segmentation map, we selected the pixel-aligned Gaussians in 3D space without optimization. This approach results in clear boundaries without additional computation and establishes a robust foundation for 3D editing.

Our contributions can be summarized as follows:

- We first propose a novel method for reconstructing an entire 3D scene with a single forward step from omnidirectional images.
- By employing a quasi-uniform grid to reduce distortion and ensure uniform sampling, we successfully address the challenges associated with distortions near the poles in omnidirectional images, achieving higher reconstruction accuracy compared to existing methods.
- We enhance multi-view consistency in pixel-level segmentation maps by leveraging attention features from the splat network, improving the accuracy and editability of the reconstructed scenes.

## 2. Related works

**Sparse view scene reconstruction and synthesis.** The advent of Neural Radiance Fields (NeRF) [22] and 3D Gaussian Splatting (3DGS) [18] has greatly advanced the field of novel view synthesis and 3D reconstruction, achieving high fidelity in scene representation when dense input views are available. However, capturing extensive views is often impractical in real-world settings, leading to growing interest in sparse-view approaches that aim to reconstruct from only a few input images. The introduction of pixel-NeRF [33] marked a pivotal moment in sparse view setting, showing the advantages of feed-forward networks in terms of inference speed and the ability to leverage large-scale datasets. Consequently, various efforts have extended feed-forward paradigms to 3DGS-based methods by regressing Gaussian parameters from pixel-aligned features [2, 4, 29]. Despite these advancements, current methods predominantly focus on conventional perspective images, limiting their application in scenarios where comprehensive scene capture is essential. In this work, we present a novel feed-forward architecture tailored for sparse omnidirectional images, enabling fast and accurate 3D scene reconstructions from limited inputs. Our approach addresses the challenges of distortion inherent to omnidirectional projections and demonstrates improved performance and computational efficiency over conventional methods.

**3D editing.** Recent 3DGS editing methods [3, 27, 32, 35] have shown remarkable performance improvements, enabling more sophisticated and efficient handling of tasks such as object addition, removal, and modification in 3DGS. Ye et al. propose Gaussian grouping [32], enabling simultaneous 3D reconstruction and segmentation through 2D mask predictions and 3D spatial consistency constraints. Wang et al. [27] propose to use text-based instructions for precise edits, while Chen et al. [3] enhance efficiency with hierarchical 3DGS and 3D inpainting. TIP-Editor [35] combines text, image prompts, and 3D bounding boxes for detailed control over target appearance while preserving the background. However, existing editing methods require extensive time for optimization and often result in elongated 3DGS, leading to imprecise boundaries when objects are modified. In contrast, OmniSplat employs pixel-based Gaussians, allowing for cleaner edits with seamless boundary transitions.

**Omnidirectional coordinate systems.** Inspired by the success of deep learning in visual scene recognition, recent studies have been extended to omnidirectional images, focusing initially on equirectangular projection (ERP) [10, 19, 26] and fisheye representations. ERP provides a simple, rectangular mapping of the sphere, but introduces severe distortions at the poles, creating inconsistencies in feature extraction. Fish-eye projection reduces distortion at the center of the view but experiences radial stretching at the edges, limiting its utility for consistent omnidirectional representation.

To mitigate these issues, quasi-uniform coordinate systems like icosahedral [7], cubed-sphere [23], and Yin-Yang grids [17] have been introduced, aiming to better balance feature distribution. The icosahedral projection divides the sphere into 20 triangular facets, achieving near-uniform distribution but complicating compatibility with CNNs due to its triangular structure. Cubed-sphere projection aligns more closely with CNNs by dividing the sphere into six square faces, which eases integration but leads to boundary discontinuities at cube edges. In contrast, the Yin-Yang grid offers an optimal solution with two overlapping square grids that cover the sphere in a quasi-uniform manner. This structure ensures smooth transitions and seamless coverage across the sphere, minimizing both polar distortion and boundary discontinuities present in other methods. Additionally, its square grid design makes it directly compatible with standard CNN operations, enabling effective feature extraction without requiring complex transformations. In this paper, we utilize the Yin-Yang grid to capture consistent spatial relationships vital for high-quality omnidirectional scene reconstruction and editing.

### 3. Method

Omnisplat aims to generate a novel-view omnidirectional image by estimating 3D Gaussian splatting from the two ref-

erence omnidirectional images. The model receives two reference omnidirectional images and the corresponding poses, which we denote them as  $\{(\mathbf{I}_i, \mathbf{P}_i)\}_{i=1,2}$ . Each image,  $\mathbf{I}_i$ , has  $H \times W \times 3$  dimension, where the width of the image is twice the height. Given the two images, OmniSplat estimates the parameters of 3D Gaussians ( $\{\mu_j, \Sigma_j, \alpha_j, c_j\}$ ) in a pixel-aligned-manner. Here, each component indicates the position, covariance, opacity and spherical harmonics coefficients of  $j$ -th Gaussian. Feed-forward networks usually generate Gaussians in a pixel-aligned manner, so each Gaussian is located near the ray vector that starts from the camera origin and passes by the corresponding pixel. After the estimation, the novel view image is rasterized from the 3DGS when the target pose is given.

Omnidirectional images have the advantage of being able to capture the entire scene in a single image. However, since omnidirectional images have different optical characteristics from pinhole images, simply applying an omnidirectional image to a model trained with perspective images produces undesirable results. For example, the Gaussians estimated from an omnidirectional image are relatively densely located in the pole region since the equirectangular projection has a higher sampling frequency at the pole. At this time, if the area where the Gaussians are distributed relatively sparsely is sampled at a high frequency in the novel view, artifacts in which bright and dark areas alternately appear will occur. One simple way to cope with the challenge is to directly train a feed-forward network for omnidirectional images, but it is difficult to obtain a training set with a large number of omnidirectional image sequences and their corresponding camera matrices.

In this work, we propose an effective method to make up for the domain gap between omnidirectional and perspective images while exploiting the knowledge of the model trained by a large number of perspective image sequences. In Section 3.1, we introduce Yin-Yang grid to decompose the omnidirectional image into two images and calculate the attention between the two domains. Also, two rasterizers for a new domain are proposed to render the estimated 3D Gaussians for the Yin and Yang grid, respectively. Section 3.2 propose an advanced segmentation and editing strategy for 3D Gaussian splatting, by improving the consistency of segments among the multiple views.

#### 3.1. Decomposing the sphere with Yin-Yang Grid with Cross Attention

**Decomposition based on Yin-Yang grid.** Although the equirectangular projection provides a one-to-one mapping from the sphere to the omnidirectional image, the varying sampling ratio according to the latitude of the image makes the characteristics of omnidirectional images different from those of perspective images. Thus, applying omnidirectional images directly to a model trained with perspective images

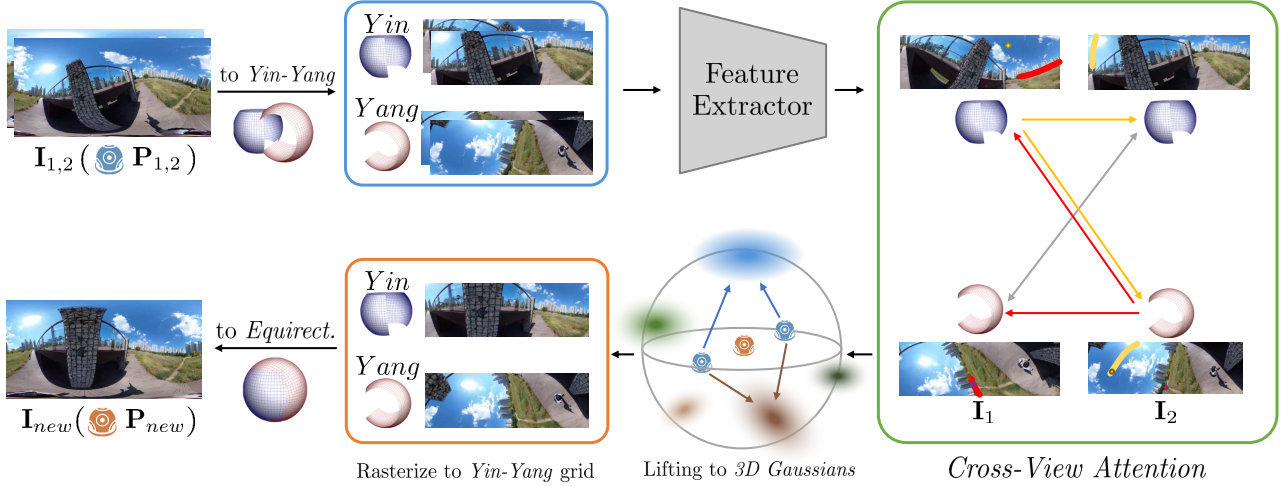


Figure 2. **The overall process of OmniSplat.** The two reference omnidirectional images are decomposed into Yin-Yang images, and the cross-view attention is conducted across grids along with epipolar lines to compose cost volume. The 3DGS parameters are estimated and Yin-Yang images are rasterized from the novel view. The two images are combined to synthesize the final omnidirectional image. In cross-view attention, we present red and yellow points and the corresponding sphere sweep curves with the same color. Each image performs cross-attention to the Yin-Yang images from other views, following geometric constraints.

causes performance degradation due to domain shift. To circumvent the challenge, we decompose the omnidirectional images into two images using Yin-Yang coordinates [17]. The Yin grid is defined as the following equations:

$$Yin = (\theta \in [-\pi/4, \pi/4]) \cap (\phi \in [-3\pi/4, 3\pi/4]), \quad (1)$$

where  $\theta$  and  $\phi$  indicate the sphere’s elevation and azimuth. The Yang grid image is computed using the same range (Eq. (1)) as the Yin grid image after rotating the sphere using matrix  $M$ . The transformation matrix is defined as follows:

$$\begin{pmatrix} x_{Yang} \\ y_{Yang} \\ z_{Yang} \end{pmatrix} = M \begin{pmatrix} x_{Yin} \\ y_{Yin} \\ z_{Yin} \end{pmatrix} = \begin{pmatrix} -1 & 0 & 0 \\ 0 & 0 & 1 \\ 0 & 1 & 0 \end{pmatrix} \begin{pmatrix} x_{Yin} \\ y_{Yin} \\ z_{Yin} \end{pmatrix}. \quad (2)$$

We denote the decomposed Yin-grid image as  $I_i^n \in \mathbb{R}^{H_n \times W_n \times 3}$  and the Yang-grid image as  $I_i^e \in \mathbb{R}^{H_e \times W_e \times 3}$ . We note that the width of  $I_i^n$  is 3 times its height, and it becomes the opposite in  $I_i^e$ .

We rotate  $I_{e,s}$  by 90 degrees to match the spatial size of  $I_{n,s}$ . Then we concatenate the total four images ( $I_n^1, I_e^1, I_n^2, I_e^2$ ) to make it look like four view images.

**Yin-Yang cross-view attention.** Following MVSpLat [4], we put all the decomposed images into the Transformer to generate features across Yin and Yang images. From the features, we generate the cost volume along depth using a Yin-Yang sweeping, an omnidirectional version of plane sweeping approach [8, 11, 16, 31]. To implement the Yin-Yang sweeping, we define omnidirectional cost volume for

each feature, warp the feature from one reference view to the other, and compute the appropriate depth value for each pixel in the feature. First, we sample a list of depth candidates where the elements compose a harmonic sequence from  $d_{near}$  to  $d_{far}$ , the pre-defined near and far distance values. Using the depth candidates, we warp the feature of one reference view to the pose of the other view. We assume that we warp the Transformer features from pose  $P_2$  (source) to pose  $P_1$  (target). The extracted features are denoted as  $F_2^n$  and  $F_2^e$ , which are generated from  $I_2^n$  and  $I_2^e$ , respectively. Since we also have two features for  $I_1$ , the warping should be processed four times to calculate the attention across all domains. Also, we compute warped masks that indicate the validity of the warping since there are cases where the query point is outside the frustum of the original image when warped.

$$F_{2 \rightarrow 1}^{j \rightarrow i}, M_{2 \rightarrow 1}^{n \rightarrow n} = \mathcal{W}_i(F_1^j, P_1, P_2), \quad (3)$$

Here,  $i, j \in \{n, e\}$  indicates the grid type (Yin, Yang) of the target and the source images, respectively. Each warped feature ( $F_{2 \rightarrow 1}$ ) has shape  $H_F \times W_F \times F \times D$ , where  $H_F, W_F, F$  are the height, width, and the number of channels of the feature, and  $D$  is the number of depth candidates. For masks, the value of the mask is set to 1 if the corresponding position is within the image frustum when viewed from  $P_2$ , and 0 otherwise. The final warped feature for each grid is mixed according to the mask:

$$F_{2 \rightarrow 1}^i = \frac{1}{M^n} (F_{2 \rightarrow 1}^{n \rightarrow i} \odot M_{2 \rightarrow 1}^{n \rightarrow i} + F_{2 \rightarrow 1}^{e \rightarrow i} \odot M_{2 \rightarrow 1}^{e \rightarrow i}), \quad (4)$$

$$M^i = M_{2 \rightarrow 1}^{n \rightarrow i} + M_{2 \rightarrow 1}^{e \rightarrow i},$$



where  $\odot$  denotes the element-wise multiplication. From Eqs. (3) and (4), the Yin and Yang features of each reference view are warped to the results from different poses without loss of features. This solves the threat of not being able to refer to values across grids that can occur with Yin-Yang decomposition.

By calculating the dot product between the warped feature and the corresponding original feature, we calculate the correlation (cross-view attention) and estimate the depth according to the correlation values.

$$\mathbf{C}_1^{\{n,e\}} = \frac{1}{\sqrt{F}} \mathbf{F}_1^{\{n,e\}} \cdot_C \mathbf{F}_{2 \rightarrow 1}^{\{n,e\}}, \quad (5)$$

where  $\cdot_C$  is a dot product along the channel axis of the feature. After the cost volumes for Yin and Yang images are constructed, we follow the other feed-forward network [4] to estimate the parameters of 3DGS.

**Rasterizer for Yin-Yang grid.** It is necessary to rasterize the predicted 3D Gaussian splatting into a 2D image in order to utilize it for novel view synthesis. However, the rasterizer of the original 3DGS work [18] can only generate perspective images, which cannot include the whole scene in one image. The rasterizer proposed by [14, 21] successfully renders the omnidirectional images from 3D Gaussian splatting, but it often creates artifacts when applied to 3DGS estimated by feed-forward networks. To solve this challenge, we propose Yin-Yang rasterizers that fit the Yin-Yang grid with quasi-uniform properties. The quasi-uniform nature of rasterization keeps the rasterized image from generating dot-shaped artifacts which occurs in omnidirectional rasterizer. After the two Yin-Yang images are rasterized, they are combined into an omnidirectional image in pixel space.

### 3.2. Gaussian Segmentation for Editing

To facilitate 3D editing in the result Gaussians, we first construct multi-view consistent segmentation maps using the cross-attention scores. Initially, we independently estimate semantic segmentation leverage on the state-of-the-art model for each reference view image. The resulting segmentation maps, however, exhibit inconsistencies in both labels and segmented regions. To address this, we establish matching between the segments across the images based on the attention scores, thereby aligning the labels and ensuring consistency. Each pixel in a reference view image is matched with the top-K pixels from the other image, as determined by cross-attention scores. Based on this matching, pixels within a segment in one image cast votes for corresponding segments in other images. A segment is then matched to the one receiving the most votes. Each segment is associated with a single match, which is consolidated through a merging process based on the directional graph.

The resulting multi-view consistent segmentation labels are then assigned to corresponding pixel-aligned Gaussians. This approach facilitates fast, feed-forward 3D segmentation by eliminating the need for additional grouping optimization in 3D. As a result, selection operations are enabled, allowing users to choose regions by selecting Gaussians with the same label. Unlike optimization-based methods, pixel-aligned Gaussians provide cleaner boundary separation.

## 4. Experiments

**Datasets.** We use six benchmark omnidirectional videos for comparing the reconstruction quality. OmniBlender [6] consists of 11 synthetic videos where each 3D scene is generated and rendered by Blender engine [9]. We use 25 test images, which are uniformly sampled from each video for each scene. Ricoh360 [6] contains 12 videos captured in outdoor scenes using real 360-degree cameras. Each scene has 50 test images that are used for comparing our method with other baselines. OmniPhotos [1] captured 10 real-world outdoor videos by rotating the 360-degree camera in a circle. Each scene consists of 71 to 91 images, and we uniformly sample 20% of images as test views for the comparison. While the aforementioned three datasets have small camera displacement between frames, we also compare our model with the other three benchmarks with large motions: 360Roam [13], OmniScenes [20] and 360VO [12].

For all datasets, we run OpenMVG [24] to obtain poses for each image since there is no pose given in the dataset. Also, We downsample all images into  $1024 \times 512$  using bicubic downsampling for all scenes.

**Metrics.** For evaluation, we use three metrics to compare the quality of test view images: PSNR, SSIM, and LPIPS. PSNR and SSIM [28] are popularly used metrics to indicate restoration accuracy. LPIPS [34] is a well-known metric to measure the perceptual quality of the output compared to the ground truth. We use VGG [25] backbone for computing the distance between the features when calculating LPIPS.

**Experimental details.** Since all datasets are not proposed for 3D reconstruction from a few inputs, we designate two new image indices to be used as reference views. For three egocentric datasets (OmniBlender, Ricoh360, and OmniPhotos), we select two indices as reference views for each scene where the two images are taken from a distance to minimize the area of occluded regions. On the contrary, for the rest three datasets (360Roam, OmniScenes, and 360VO), the camera movement distance between adjacent frames is long, so the overlap ratio between frames is low. Therefore, we set two frames with an interval of 4 to 5 timesteps as reference images and designated the frames in between as test views to compare the restoration performance. The detailed indices for the reference views and test views are written in the supplementary materials. The parameters of the feed-forward 3DGS estimation part of OmniSplat are loaded brought from

Dataset		OmniBlender			Ricoh360			OmniPhotos		
Methods	Runtime (s)	PSNR $\uparrow$	SSIM $\uparrow$	LPIPS $\downarrow$	PSNR $\uparrow$	SSIM $\uparrow$	LPIPS $\downarrow$	PSNR $\uparrow$	SSIM $\uparrow$	LPIPS $\downarrow$
PixelSplat (P) [2]	13.068	20.56	0.6562	<u>0.3222</u>	19.36	<b>0.6307</b>	0.3626	<b>19.94</b>	<u>0.6486</u>	<b>0.3119</b>
LatentSplat (P) [29]	16.097	17.28	0.5523	0.4361	16.89	0.4113	0.5927	16.30	0.5389	0.4386
MVSplat (P) [4]	2.224	17.48	0.5593	0.4385	18.99	0.6394	0.3726	18.12	0.5947	0.3804
PixelSplat (O) [2]	2.045	16.97	0.3837	0.5967	17.06	0.3878	0.5539	16.44	0.3546	0.5810
MVSplat (O) [4]	<u>0.832</u>	16.97	0.5635	0.3949	15.68	0.4880	0.4524	15.89	0.5478	0.4049
OmniSplat	<b>0.532</b>	<u>21.02</u>	<u>0.6691</u>	0.3231	<u>19.70</u>	0.6104	<u>0.3598</u>	18.50	0.6311	0.3794
OmniSplat+ <i>opt</i>	12.04	<b>22.33</b>	<b>0.6994</b>	<b>0.2879</b>	<b>20.36</b>	<u>0.6288</u>	<b>0.3303</b>	<u>19.63</u>	<b>0.6608</b>	<u>0.3217</u>
ODGS [21]	1920	22.23	0.6807	0.3124	17.51	0.5309	0.3911	20.25	0.5660	0.3730

Dataset		360Roam			OmniScenes			360VO		
Methods		PSNR $\uparrow$	SSIM $\uparrow$	LPIPS $\downarrow$	PSNR $\uparrow$	SSIM $\uparrow$	LPIPS $\downarrow$	PSNR $\uparrow$	SSIM $\uparrow$	LPIPS $\downarrow$
PixelSplat (P) [2]		16.31	0.5270	<u>0.4415</u>	19.88	0.7193	0.3502	19.33	0.6628	0.3079
LatentSplat (P) [29]		15.58	0.5315	0.4731	17.04	0.6907	0.3998	18.36	0.6457	0.3345
MVSplat (P) [4]		15.96	0.5249	0.4930	19.06	0.6954	0.3710	19.19	0.6322	0.3118
PixelSplat (O) [2]		14.87	0.2614	0.6430	17.58	0.4152	0.6082	17.79	0.4635	0.5411
MVSplat (O) [4]		12.58	0.3680	0.5221	13.68	0.7202	0.3635	17.45	0.6695	0.2991
OmniSplat		<u>17.88</u>	<u>0.5366</u>	0.4597	<u>22.87</u>	<u>0.7938</u>	<u>0.2860</u>	<u>20.07</u>	<u>0.7225</u>	<u>0.2618</u>
OmniSplat+ <i>opt</i>		<b>18.27</b>	<b>0.5570</b>	<b>0.4226</b>	<b>24.17</b>	<b>0.8146</b>	<b>0.2570</b>	<b>20.94</b>	<b>0.7453</b>	<b>0.2357</b>
ODGS [21]		18.72	0.5630	0.3833	20.71	0.7598	0.2749	22.66	0.7786	0.2222

Table 1. **Quantitative comparison.** Reconstructed results in novel view omnidirectional images with existing feed-forward networks and an optimization-based approach on various datasets. The best and the second best scores among feed-forward methods are written in **bold** and underlined, respectively.

the pre-trained model of MVSplat [4].

#### 4.1. Novel View Synthesis

To the best of our knowledge, no works estimate the whole 3D Gaussian splatting from a few multi-view omnidirectional images. Thus, we changed the dataset format and transformed some functions of the model to correspond to omnidirectional images, and then compared them with OmniSplat. Table 1 shows the quantitative results for the test view images according to the synthesis methods.

First, PixelSplat [2], LatentSplat [29], and MVSplat [4] are designed to generate parameters of 3D Gaussian splatting from a few perspective images. However, their models only support perspective images and cannot be used for omnidirectional images. To use those models as baselines, we decompose each input omnidirectional image into six perspective images using cubemap decomposition. Cubemap decomposition draws a virtual cube that touches the unit sphere and then creates six perspective images and the corresponding poses where each face is considered a camera plane. Then, 12 perspective images are put into the network, generating six perspective images for the test camera pose, and they are combined with the omnidirectional image. Since PixelSplat and LatentSplat cannot receive more than two images, we choose one image per view, construct a set of 36 pair products, and unify all Gaussians for each

pair. Then, the omnidirectional image is synthesized from six rasterized cubemap images. For those cases, we write ‘(P)’ after the model names in the method to indicate that the model is executed with the perspective images. Compared to OmniSplat, perspective feed-forward models take a much longer time to generate the output. This is because it takes a long time to compute cross-attention between 12 images or predict Gaussians of 36 pairs, and it also takes time to warp 6 cubemap images to stitch them. Reconstruction performance is measured lower than OmniSplat except for PixelSplat, as features were mixed with too many views or too many Gaussians were unified.

Meanwhile, we modify some functions of PixelSplat and MVSplat, which calculate the ray direction according to the projection on the image pixel or the camera plane, to fit the optical characteristics of equirectangular projection so that they can be applied to omnidirectional images. After creating 3DGS, we directly synthesize novel view omnidirectional image using omnidirectional rasterizer [21]. The character ‘(O)’ after the model names indicates that the omnidirectional version of the model is utilized. Although these models showed faster generation speeds than the perspective versions, the quality of the generated results was measured to be worse. We speculate that this happens because the feature extractor trained on perspective images fails to obtain appropriate features with omnidirectional images and



Figure 3. **Qualitative comparison.** Novel view synthesized image examples in various datasets. Each scene is brought from OmniBlender, Ricoh360, and OmniPhotos, respectively. *Best viewed when zoomed in.*

because of the dense sampling in the polar regions of the equirectangular projection.

ODGS [21] is an optimization-based 3DGS estimation method specifically designed for omnidirectional images. In the experiment, we measure the performance after 30,000 iterations of optimization for each scene, which takes about 30 minutes. Despite including the optimization process for each scene, the results do not outperform those of the feed-forward networks and even show worse results in some scenes. This phenomenon occurs because overfitting often occurs during optimization with only two reference images; ODGS shows the best results in reference views, but the image is completely broken when rendered in novel views.

OmniSplat shows the best results for most settings, demonstrating the power of the Yin-Yang decomposition and the corresponding rasterizer with the fastest rendering speed. Furthermore, we present ‘OmniSplat+*opt*’, after a small amount of optimization of the color and opacity properties in 3DGS with reference views. Different from ODGS, our method is much more robust to overfitting since 3DGS predicted by OmniSplat serve as good initialization points, and their positions are not updated during optimization. While reporting similar runtime to PixelSplat (P), OmniSplat+*opt* shows better performance in the majority of datasets.

The novel-view synthesized images according to 3DGS reconstruction methods on various datasets are illustrated in Figure 3. Despite reporting decent metrics, images synthesized by ODGS contain many artifacts since the Gaussians are overfitted to the reference views, generating wrong re-

sults in novel viewpoints. PixelSplat (P), despite reporting comparable quantitative performance, produces misaligned and blurry images due to the overlapping of Gaussians made from many perspective pairs. Additionally, if the image only has simple textures, such as the sky and walls, it may not be able to create meaningful features, leading to incorrect depth estimation and inaccurate restoration results. In the case of MVSSplat (O), the overall tone of the photo appears darker than the ground truth. Also, dot-shaped artifact patterns occur frequently at the top and bottom of the image. This artifact occurs because the Gaussians located in 3D space are not dense or large enough to produce an accurate pattern when rasterized with the high sampling rate at the pole regions. Consequently, some pixels appear bright as they pass through a Gaussian, while other areas appear dark due to insufficient coverage. Our method, OmniSplat, generates the most accurate and photo-realistic images compared to previous methods.

## 4.2. Gaussian Segmentation and Editing

We obtain multi-view-consistent semantic segmentation for semantic-based Gaussian selection. We compare our attention-based matching approach with the segmentation tracking method DEVA [5] as illustrated in Figure 4. In Figure 4a and Figure 4c, the selected points from the source view are marked with stars of different colors. Regions sharing the same label as the selected points are highlighted with corresponding color masks. Figure 4b and Figure 4d depict how these regions correspond in the target view upon



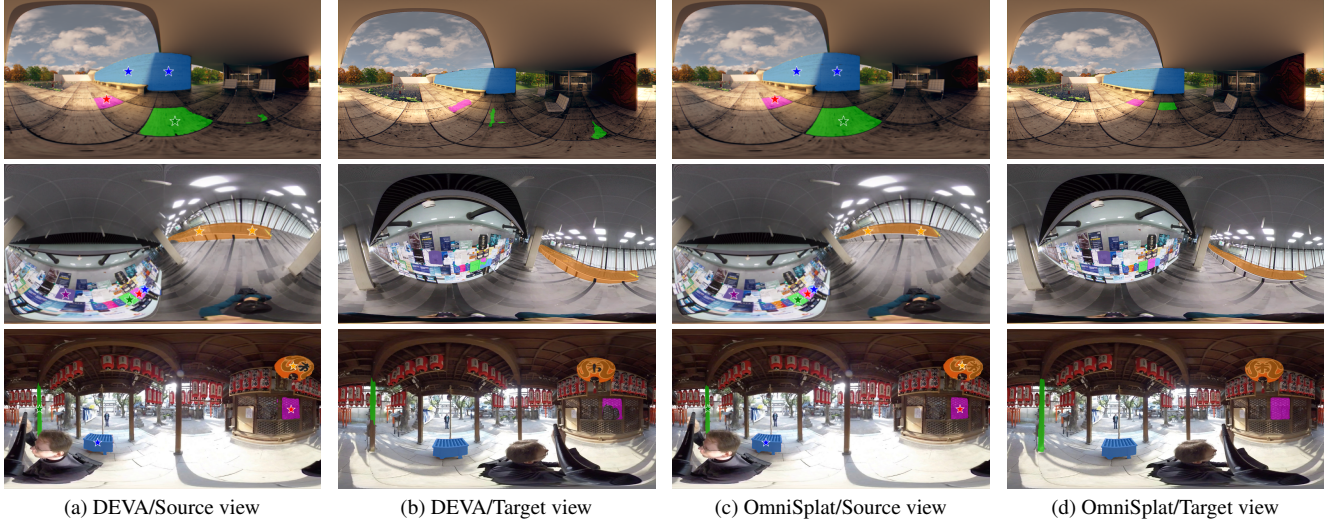


Figure 4. **Visualization of object segmentation.** We visualize the matched segments among the source and the target views. The stars in the image indicate query points for the user to segment objects containing the stars.

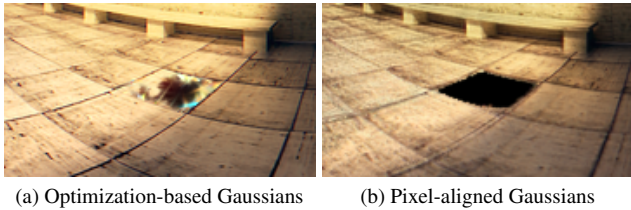


Figure 5. **Example of Gaussian removal results in the object segment.** Compared to (a), where overlapping Gaussians result in incomplete removal, (b) pixel-aligned Gaussians offer clear edges that are advantageous for editing.

the tracking-based method and our attention-based method. DEVA, a video tracking-based method, shows some tracking failures when the camera moves significantly, resulting in the disappearance or mixing of regions identified in the source view. In contrast, our approach demonstrated in Figure 4d achieves multi-view-consistent segmentation. Notably, we identify matched segments based on attention scores obtained during the reconstruction process, which enable the retrieval of corresponding segmentation regions without additional computation.

Upon this multi-view matched segments, we select the semantic Gaussians in a view-consistent manner and utilize them for editing. Figure 5 illustrates the result of removing 3D Gaussians selected based on the multi-view segmentation regions. The removal result with the Gaussians optimized as 3DGS is illustrated in Figure 5a. Since the optimized Gaussians tend to have elongated shapes [15, 30, 32], the selected regions are not cleanly removed, often resulting in needle-like artifacts. In contrast, our method with the pixel-aligned Gaussians provides clear boundaries, enabling a cleaner removal operation and establishing a solid foundation for subsequent operations such as image inpainting.

## 5. Conclusion

In this work, we propose OmniSplat, a pioneering work for a feed-forward 3D scene reconstruction from omnidirectional images. Although omnidirectional images have a wide field-of-view that can capture the entire scene in a single frame, existing feed-forward models [2, 4, 29] cannot be used with omnidirectional images due to the difference of optical characteristics from perspective images. Specifically, optical distortion at the edges of an omnidirectional image can force the model to extract incorrect features, and non-uniformly generated Gaussians often create artifacts during rendering. To cope with the issues, we introduce Yin-Yang grid, which can represent spheres in a quasi-uniform manner while having a typical lattice structure. The two decomposed images and the corresponding features are warped with cross-view attention to estimate the depth of each pixel and parameters of 3DGS. The proposed Yin-Yang rasterizer successfully renders the Yin-Yang images at the query view, which are combined in image space to synthesize the omnidirectional image. OmniSplat shows more accurate and visually pleasing reconstruction results than previous feed-forward networks designed for perspective images while reporting faster inference speed.

**Limitations and future works.** Although OmniSplat shows superiority in rendering novel view omnidirectional images, there is some room for further improvement. First, when transforming a Yang image to an omnidirectional domain, interpolation is required in the horizontal direction, which reduces the quality of the image. Also, although 3DGS has been improved through hundreds of adaptations, we believe that the adaptation steps can be further reduced through meta-learning, *etc.*



## References

- [1] Tobias Bertel, Mingze Yuan, Reuben Lindroos, and Christian Richardt. Omniphotos: casual 360 vr photography. *ACM TOG*, 2020. 5, 10
- [2] David Charatan, Sizhe Lester Li, Andrea Tagliasacchi, and Vincent Sitzmann. Pixelsplat: 3d gaussian splats from image pairs for scalable generalizable 3d reconstruction. In *CVPR*, 2024. 1, 2, 6, 7, 8, 11
- [3] Yiwen Chen, Zilong Chen, Chi Zhang, Feng Wang, Xiaofeng Yang, Yikai Wang, Zhongang Cai, Lei Yang, Huaping Liu, and Guosheng Lin. Gaussianeditor: Swift and controllable 3d editing with gaussian splatting. In *CVPR*, 2024. 3
- [4] Yuedong Chen, Haofei Xu, Chuanxia Zheng, Bohan Zhuang, Marc Pollefeys, Andreas Geiger, Tat-Jen Cham, and Jianfei Cai. Mvsplat: Efficient 3d gaussian splatting from sparse multi-view images. In *ECCV*, 2024. 1, 2, 4, 5, 6, 7, 8, 11
- [5] Ho Kei Cheng, Seoung Wug Oh, Brian Price, Alexander Schwing, and Joon-Young Lee. Deva: Tracking anything with decoupled video segmentation. In *ICCV*, 2023. 7
- [6] Changwoon Choi, Sang Min Kim, and Young Min Kim. Balanced spherical grid for egocentric view synthesis. In *CVPR*, 2023. 1, 5, 10
- [7] Taco Cohen, Maurice Weiler, Berkay Kicanaoglu, and Max Welling. Gauge equivariant convolutional networks and the icosahedral cnn. In *ICML*, 2019. 2, 3
- [8] Robert T Collins. A space-sweep approach to true multi-image matching. In *CVPR*, 1996. 4
- [9] Blender Online Community. *Blender - a 3D modelling and rendering package*. Blender Foundation, Stichting Blender Foundation, Amsterdam, 2018. 5
- [10] Benjamin Coors, Alexandru Paul Condurache, and Andreas Geiger. Spherenet: Learning spherical representations for detection and classification in omnidirectional images. In *ECCV*, 2018. 3
- [11] Hyowon Ha, Sunghoon Im, Jaesik Park, Hae-Gon Jeon, and In So Kweon. High-quality depth from uncalibrated small motion clip. In *CVPR*, 2016. 4
- [12] Huajian Huang and Sai-Kit Yeung. 360vo: Visual odometry using a single 360 camera. In *ICRA*, 2022. 5, 10
- [13] Huajian Huang, Yingshu Chen, Tianjia Zhang, and Sai-Kit Yeung. Real-time omnidirectional roaming in large scale indoor scenes. In *SIGGRAPH Asia 2022 Technical Communications*, 2022. 5, 10
- [14] Letian Huang, Jiayang Bai, Jie Guo, Yuanqi Li, and Yanwen Guo. On the error analysis of 3d gaussian splatting and an optimal projection strategy. In *ECCV*, 2024. 5
- [15] Junha Hyung, Susung Hong, Sungwon Hwang, Jaeseong Lee, Jaegul Choo, and Jin-Hwa Kim. Effective rank analysis and regularization for enhanced 3d gaussian splatting. *arXiv preprint arXiv:2406.11672*, 2024. 8
- [16] Sunghoon Im, Hae-Gon Jeon, Stephen Lin, and In So Kweon. Dpsnet: End-to-end deep plane sweep stereo. In *ICLR*, 2019. 4
- [17] Akira Kageyama and Tetsuya Sato. “yin-yang grid”: An overset grid in spherical geometry. *Geochemistry, Geophysics, Geosystems*, 5(9), 2004. 2, 3, 4
- [18] Bernhard Kerbl, Georgios Kopanas, Thomas Leimkühler, and George Drettakis. 3d gaussian splatting for real-time radiance field rendering. *ACM TOG*, 2023. 1, 2, 5
- [19] Renata Khasanova and Pascal Frossard. Graph-based classification of omnidirectional images. In *ICCV*, 2017. 3
- [20] Junho Kim, Changwoon Choi, Hojun Jang, and Young Min Kim. Piccolo: Point cloud-centric omnidirectional localization. In *CVPR*, 2021. 5, 10
- [21] Suyoung Lee, Jaeyoung Chung, Jaeyoo Huh, and Kyoung Mu Lee. Odgs: 3d scene reconstruction from omnidirectional images with 3d gaussian splattings. *arXiv preprint arXiv:2410.20686*, 2024. 2, 5, 6, 7, 10
- [22] Ben Mildenhall, Pratul P. Srinivasan, Matthew Tancik, Jonathan T. Barron, Ravi Ramamoorthi, and Ren Ng. Nerf: Representing scenes as neural radiance fields for view synthesis. In *ECCV*, 2020. 2
- [23] Rafael Monroy, Sebastian Lutz, Tejo Chalasani, and Aljosa Smolic. Salnet360: Saliency maps for omni-directional images with cnn. *Signal Processing: Image Communication*, 2018. 2, 3
- [24] Pierre Moulon, Pascal Monasse, Romuald Perrot, and Renaud Marlet. OpenMVG: Open multiple view geometry. In *RRPR*, 2016. 5, 10
- [25] Karen Simonyan and Andrew Zisserman. Very deep convolutional networks for large-scale image recognition. In *ICLR*, 2015. 5
- [26] Yu-Chuan Su and Kristen Grauman. Learning spherical convolution for fast features from 360° imagery. In *NeurIPS*, 2017. 3
- [27] Junjie Wang, Jiemin Fang, Xiaopeng Zhang, Lingxi Xie, and Qi Tian. Gaussianeditor: Editing 3d gaussians delicately with text instructions. In *CVPR*, 2024. 3
- [28] Zhou Wang, Alan C Bovik, Hamid R Sheikh, Eero P Simoncelli, et al. Image quality assessment: From error visibility to structural similarity. *IEEE TIP*, 2004. 5
- [29] Christopher Wewer, Kevin Raj, Eddy Ilg, Bernt Schiele, and Jan Eric Lenssen. latentsplat: Autoencoding variational gaussians for fast generalizable 3d reconstruction. In *ECCV*, 2024. 1, 2, 6, 8
- [30] Tianyi Xie, Zeshun Zong, Yuxing Qiu, Xuan Li, Yutao Feng, Yin Yang, and Chenfanfu Jiang. Physsgaussian: Physics-integrated 3d gaussians for generative dynamics. In *CVPR*, 2024. 8
- [31] Ruigang Yang and Marc Pollefeys. Multi-resolution real-time stereo on commodity graphics hardware. In *CVPR*, 2003. 4
- [32] Mingqiao Ye, Martin Danelljan, Fisher Yu, and Lei Ke. Gaussian grouping: Segment and edit anything in 3d scenes. In *ECCV*, 2024. 3, 8
- [33] Alex Yu, Vickie Ye, Matthew Tancik, and Angjoo Kanazawa. pixelNeRF: Neural radiance fields from one or few images. In *CVPR*, 2021. 2
- [34] Richard Zhang, Phillip Isola, Alexei A. Efros, Eli Shechtman, and Oliver Wang. The unreasonable effectiveness of deep features as a perceptual metric. In *CVPR*, 2018. 5
- [35] Jingyu Zhuang, Di Kang, Yan-Pei Cao, Guanbin Li, Liang Lin, and Ying Shan. Tip-editor: An accurate 3d editor following both text-prompts and image-prompts. In *ACM TOG*, 2024. 3

# OmniSplat: Taming Feed-Forward 3D Gaussian Splatting for Omnidirectional Images with Editable Capabilities

## Supplementary Material

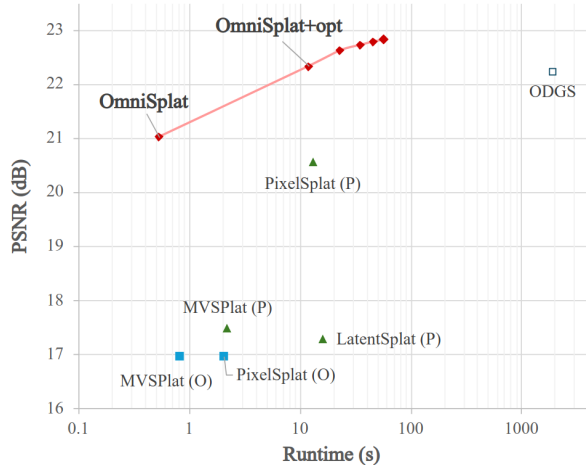


Figure A. **PSNR-runtime trade-off.** A chart of reconstruction performance-runtime trade-off in novel view image on OmniBlender [6] including the ablation according to the number of optimizations.

### A. Details on OmniSplat+opt

As briefly mentioned in Section 4.1, we add a small number of optimizations for each scene using the reference view images for fast performance improvement and call the method ‘OmniSplat+opt.’ Compared to ODGS [21], the optimization process of OmniSplat+opt is different in many aspects. First, while ODGS starts optimization from the sparse point cloud estimated by OpenMVG [24], our model starts from 3D Gaussians generated by OmniSplat, which contains much more information. Next, we set the number of optimization steps of OmniSplat+opt to 100, whereas ODGS optimizes 30,000 times. Since OmniSplat’s initial points are highly accurate, significant performance improvement can be achieved with a small number of iterations. Thus, the optimization time only takes 11 seconds, which is more than 150 times shorter than ODGS (32 minutes). Finally, we only optimize the color (sh coefficients) and opacity properties of 3DGS and keep the position and covariance fixed since changes in position or covariance can cause overfitting when optimizing with a few images.

**Ablation Studies: number of optimizing iterations** We measure the performance of test view images according to the number of optimizing iterations, starting from the original OmniSplat. As mentioned, optimization with reference

# opt.	0	100	200	300	400	500
PSNR	21.02	22.33	22.62	22.72	22.78	<b>22.82</b>
SSIM	0.6691	0.6994	<b>0.7002</b>	0.6985	0.6963	0.6943
LPIPS	0.3233	0.2879	<b>0.2851</b>	0.2858	0.2873	0.2890
Time (s)	0	12	23	35	46	57

Table A. Changes in performance according to the number of iterations for adaptation in OmniBlender [6].

images improves performance in test view images in the earlier stage. However, if we optimize 3DGS for a long time only with the reference views, the 3DGS may be overfitted, and the performance of the test views may be saturated or even reduced. Table A shows the changes of metrics (PSNR, SSIM, and LPIPS) as well as optimization time according to the number of optimization iterations (# opt.) in OmniBlender [6]. PSNR grows rapidly at the first 100 iterations but becomes saturated as optimization proceeds. For SSIM and LPIPS, the best value is achieved after 200 iterations of optimization and gets worse when the number of iterations exceeds 200. In terms of time, the optimization takes about 11-12 seconds for 100 iterations, and the time linearly grows as the number of optimizations increases. We find out that 100 or 200 iterations are optimal for additional optimization from OmniSplat, considering both time and performance. In the main manuscript, we use 100 times optimization, which takes a similar time to PixelSplat or LatentSplat.

We illustrate the PSNR-runtime trade-off, including the values of Table A in Figure A. Compared to existing feed-forward models, OmniSplat achieves higher PSNR with the fastest running speed. Additionally, the PSNR values get higher than ODGS within a minute of optimization, which are denoted as OmniSplat+opt. From the figure, we maintain that OmniSplat achieves the best PSNR-runtime trade-off for novel view synthesis.

### B. Implementation Details and Additional Quantitative Results

We write the indices for reference and test views for each scene in Tables B to G along with detailed quantitative results. For three datasets with relatively small camera motions (OmniBlender, Ricoh360 [6], OmniPhotos [1]), we select the two reference views with large pose distances and set the rest as test views. For the other three datasets (360Roam [13], OmniScenes [20], 360VO [12]), the pose distance between two adjacent cameras is large, and we selected two frames

with 3 to 4 timestep intervals as two reference views. Then, the test view indices are composed of frames between the reference views. For example, if the reference view indices are 1 and 5, the test view indices are 2, 3, and 4.

Also, we write quantitative metrics for every scene in Tables B to G, respectively. The best result for each metric is written in **bold**, and the second best result is written in underlined. As shown in the tables, OmniSplat+*opt* shows the best or the second best results in almost all metrics. Although ODGS shows conspicuous results, ODGS still shows optimal quality-runtime tradeoff, considering that ODGS requires scene-wise optimization.

### C. Additional Qualitative Results

In Figures B to G, we provide additional qualitative comparison with more baselines on various datasets. Perspective feed-forward models, PixelSplat (P) [2] and MVSplat (P) [4], produce blurry images. For PixelSplat, Gaussians are generated for every pair among twelve perspective images, and since the positions of the Gaussians generated for each pair are slightly different, a blurry image is rendered in the novel viewpoints. For MVSplat, the encoded features and cross-attention values are averaged across all perspective images, which causes blur or ghost artifacts in novel view synthesized images. Omnidirectional feed-forward models, PixelSplat (O) and MVSplat (O), produce dark images overall and striped patterns in the upper and lower areas. We attribute the phenomenon to the non-uniform sampling of the omnidirectional grid during rasterization. ODGS sometimes shows prominent image quality, but it requires over 30 minutes of optimization for each scene. Moreover, it often falls into overfitting, generating floater artifacts that severely degrade the quality of the image. Our method, OmniSplat, produces clearer and more accurate images than other feed-forward networks and ODGS. Also, the results can be further improved with a small number of optimization (OmniSplat+*opt*), which only takes 11 seconds, which is shorter than the execution time of PixelSplat (P).

We also provide a video sample that compares our models with PixelSplat (P), MVSplat (O), and ODGS. This video was rendered with a pose sequence created by interpolating two reference views from several scenes. We can clearly see the floater artifact of ODGS, the blurriness of Pixelsplat (P), and the dark strip pattern of MVSplat (O) in this video. On the other hand, OmniSplat maintains consistently good image quality in all novel views.

Scene	Ref. view	Test view	ODGS	PixelSplat (P)	LatentSplat (P)	MVSplat (P)	PixelSplat (O)	MVSplat (O)	OmniSplat	OmniSplat+opt
archiviz-flat	14, 86	2, 6, ..., 98	22.17 / 0.7511 / 0.3188	20.93 / 0.7128 / 0.3274	18.40 / 0.6859 / 0.3981	18.35 / 0.6704 / 0.3870	17.28 / 0.4285 / 0.6206	17.73 / 0.6818 / 0.4138	23.93 / 0.8010 / 0.2688	<b>24.97 / 0.8147 / 0.2618</b>
barbershop	14, 86	2, 6, ..., 98	<b>25.01 / 0.7683 / 0.2802</b>	19.83 / 0.6243 / 0.3588	17.96 / 0.5627 / 0.4666	17.98 / 0.5636 / 0.4445	17.70 / 0.4262 / 0.6197	16.60 / 0.5214 / 0.4459	21.76 / 0.7067 / 0.3328	<b>22.70 / 0.7229 / 0.3110</b>
bistro bike	14, 86	2, 6, ..., 98	<b>21.05 / 0.6800 / 0.2687</b>	20.20 / 0.5882 / 0.2981	15.43 / 0.4248 / 0.4343	17.29 / 0.4619 / 0.4241	16.50 / 0.3613 / 0.5527	16.40 / 0.5253 / 0.3354	20.20 / 0.6312 / 0.2844	<b>21.75 / 0.6868 / 0.2459</b>
bistro square	14, 86	2, 6, ..., 98	<b>19.30 / 0.6397 / 0.3030</b>	<b>20.11 / 0.5989 / 0.2904</b>	15.43 / 0.4290 / 0.4427	16.41 / 0.4348 / 0.4376	14.93 / 0.2878 / 0.5746	13.76 / 0.4338 / 0.4070	18.43 / 0.5535 / 0.3185	<b>18.98 / 0.5845 / 0.2844</b>
classroom	14, 86	2, 6, ..., 98	<b>23.55 / 0.6436 / 0.3655</b>	20.50 / 0.6803 / 0.3112	17.46 / 0.6150 / 0.4574	16.47 / 0.6022 / 0.4719	16.61 / 0.3884 / 0.6115	16.30 / 0.5223 / 0.4130	19.01 / 0.7113 / 0.3505	<b>21.63 / 0.7264 / 0.3107</b>
fisher hut	14, 86	2, 6, ..., 98	<b>21.07 / 0.6326 / 0.3516</b>	22.75 / <b>0.7389</b> / 0.3253	19.91 / 0.6673 / 0.3773	21.08 / 0.7226 / 0.3660	18.93 / 0.4390 / 0.5900	20.90 / 0.6487 / 0.4265	25.08 / 0.7244 / 0.3155	<b>26.60 / 0.7269 / 0.2743</b>
lone monk	14, 86	2, 6, ..., 98	<b>20.21 / 0.6907 / 0.3053</b>	16.89 / 0.5907 / 0.3402	14.12 / 0.4640 / 0.4277	15.33 / 0.4947 / 0.4195	14.23 / 0.3075 / 0.6029	13.09 / 0.5371 / 0.4259	19.04 / 0.6175 / 0.2978	<b>19.28 / 0.6374 / 0.2945</b>
LOU	14, 86	2, 6, ..., 98	<b>21.53 / 0.7332 / 0.2469</b>	18.97 / 0.6801 / 0.3246	14.47 / 0.5251 / 0.4452	15.17 / 0.4348 / 0.4459	16.49 / 0.4040 / 0.5842	18.16 / 0.6678 / 0.3141	19.51 / 0.6438 / 0.3071	<b>20.33 / 0.7420 / 0.2622</b>
pavilion midday chair	14, 86	2, 6, ..., 98	21.24 / 0.6541 / 0.3516	<b>21.28 / 0.7035 / 0.3198</b>	18.29 / 0.6050 / 0.4178	18.30 / 0.6470 / 0.3868	17.06 / 0.4382 / 0.5765	16.71 / 0.5623 / 0.4193	21.02 / 0.6836 / 0.3216	<b>22.09 / 0.7005 / 0.3051</b>
pavilion midday pond	14, 86	2, 6, ..., 98	<b>19.21 / 0.4918 / 0.4229</b>	<b>19.70 / 0.6058 / 0.3353</b>	15.31 / 0.4486 / 0.5241	14.24 / 0.4348 / 0.6142	15.40 / 0.3021 / 0.6316	15.63 / 0.4752 / 0.4120	18.34 / 0.5609 / 0.3776	<b>19.18 / 0.5749 / 0.3328</b>
restroom	14, 86	2, 6, ..., 98	<b>20.21 / 0.8030 / 0.2220</b>	24.95 / 0.6947 / 0.3132	23.33 / 0.6481 / 0.4063	21.71 / 0.6551 / 0.4263	21.54 / 0.4381 / 0.5999	21.43 / 0.6229 / 0.3305	23.02 / 0.7266 / 0.3792	<b>28.17 / 0.7720 / 0.2845</b>
average	-	-	<b>22.23 / 0.6807 / 0.3124</b>	20.56 / 0.6562 / 0.3222	17.28 / 0.5523 / 0.4361	17.48 / 0.5565 / 0.4385	16.97 / 0.3837 / 0.5967	16.97 / 0.5635 / 0.3949	21.02 / 0.6691 / 0.3231	<b>22.33 / 0.6994 / 0.2879</b>

Table B. Scene-wise quantitative results of 3D reconstruction on **OmniBlender** dataset.

Scene	Ref. view	Test view	ODGS	PixelSplat (P)	LatentSplat (P)	MVSplat (P)	PixelSplat (O)	MVSplat (O)	OmniSplat	OmniSplat+opt
bricks	35, 69	1, 3, ..., 99	16.41 / 0.5116 / 0.3738	16.28 / 0.5161 / 0.4249	13.38 / 0.4586 / 0.4781	17.86 / 0.5834 / 0.3820	15.89 / 0.4091 / 0.5296	15.01 / 0.5017 / 0.4070	19.25 / 0.5980 / 0.3374	<b>19.91 / 0.6388 / 0.3052</b>
bridge	33, 57	1, 3, ..., 99	15.84 / 0.4333 / 0.4546	16.45 / 0.5264 / 0.3999	15.71 / 0.4367 / 0.5402	18.68 / 0.6120 / 0.3446	16.62 / 0.3937 / 0.5269	17.25 / 0.5947 / 0.3436	19.53 / 0.6198 / 0.3183	<b>19.53 / 0.6198 / 0.3183</b>
bridge under	23, 77	1, 3, ..., 99	15.07 / 0.4841 / 0.3916	15.78 / 0.4519 / 0.4572	14.67 / 0.4772 / 0.4473	14.24 / 0.4492 / 0.4896	15.51 / 0.3123 / 0.5839	16.08 / 0.4179 / 0.4140	18.95 / 0.5598 / 0.3572	<b>19.52 / 0.5794 / 0.3279</b>
cat tower	3, 83	1, 3, ..., 99	18.59 / 0.4641 / 0.4210	<b>20.19 / 0.7243 / 0.3186</b>	17.14 / 0.4167 / 0.6799	17.14 / 0.4167 / 0.6799	16.68 / 0.3654 / 0.5489	16.53 / 0.4640 / 0.4855	18.29 / 0.5133 / 0.4005	<b>19.42 / 0.5507 / 0.3599</b>
center	25, 49	1, 3, ..., 99	19.56 / 0.6045 / 0.3659	<b>21.61 / 0.6936 / 0.2948</b>	17.28 / 0.3716 / 0.5863	21.32 / <b>0.7594</b> / 0.3107	17.97 / 0.4407 / 0.5556	17.01 / 0.6090 / 0.3886	20.66 / 0.7094 / 0.3210	<b>21.57 / 0.7320 / 0.2887</b>
farm	83, 99	1, 3, ..., 99	18.05 / 0.5087 / 0.3431	18.31 / 0.5168 / 0.3605	16.31 / 0.4110 / 0.4937	<b>19.73 / 0.5789</b> / 0.3447	16.49 / 0.3470 / 0.5068	12.93 / 0.3631 / 0.4969	18.29 / 0.5133 / 0.3646	<b>18.56 / 0.5227 / 0.3409</b>
flower	29, 55	1, 3, ..., 99	15.37 / 0.4163 / 0.4084	<b>17.07 / 0.5179 / 0.4260</b>	16.46 / 0.4110 / 0.4992	<b>16.03 / 0.5468</b> / 0.4207	15.65 / 0.3063 / 0.5376	14.57 / 0.3507 / 0.4954	16.90 / 0.4306 / 0.4350	<b>17.46 / 0.4436 / 0.4120</b>
gallery chair	5, 23	1, 3, ..., 99	19.78 / 0.6557 / 0.3587	<b>25.12 / 0.8192 / 0.2625</b>	18.96 / 0.3871 / 0.7146	<b>22.96 / 0.7780</b> / 0.3349	19.19 / 0.4497 / 0.5694	17.62 / 0.5742 / 0.4504	22.30 / 0.7374 / 0.3264	<b>22.89 / 0.7427 / 0.3060</b>
gallery park	33, 99	1, 3, ..., 99	16.29 / 0.5766 / 0.3848	19.19 / 0.6971 / 0.3601	17.87 / 0.3470 / 0.7216	<b>19.67 / 0.7169</b> / 0.3562	18.65 / 0.4561 / 0.5442	17.54 / 0.5788 / 0.4490	19.64 / 0.6568 / 0.3670	<b>20.13 / 0.6653 / 0.3409</b>
gallery pillar	21, 39	1, 3, ..., 99	16.67 / 0.6461 / 0.3664	<b>21.80 / 0.7497 / 0.3213</b>	20.00 / 0.3621 / 0.6785	19.03 / 0.6873 / 0.3694	17.23 / 0.3913 / 0.5875	17.16 / 0.5931 / 0.4376	21.45 / 0.7052 / 0.3477	<b>22.51 / 0.7284 / 0.3048</b>
garden	31, 59	1, 3, ..., 99	18.97 / 0.5338 / 0.4027	<b>20.38 / 0.6595 / 0.3989</b>	19.22 / 0.3886 / 0.6406	<b>23.09 / 0.7193</b> / 0.3373	18.84 / 0.3943 / 0.5652	15.53 / 0.4690 / 0.4790	22.43 / 0.6335 / 0.3406	<b>22.09 / 0.6544 / 0.3052</b>
poster	51, 85	1, 3, ..., 99	16.46 / 0.5342 / 0.4219	<b>20.15 / 0.6964 / 0.3263</b>	15.72 / 0.4675 / 0.5827	<b>19.99 / 0.6179</b> / 0.4047	16.01 / 0.3879 / 0.5911	14.36 / 0.4897 / 0.4582	18.71 / 0.6517 / 0.3761	<b>19.36 / 0.6674 / 0.3551</b>
average	-	-	17.51 / 0.5309 / 0.3911	19.36 / 0.6307 / 0.3626	16.89 / 0.4113 / 0.5927	18.99 / 0.6394 / 0.3726	17.06 / 0.3878 / 0.5539	15.68 / 0.4880 / 0.4524	19.70 / 0.6104 / 0.3598	<b>20.36 / 0.6288 / 0.3303</b>

Table C. Scene-wise quantitative results of 3D reconstruction on **Ricoh360** dataset.

Scene	Ref. view	Test view	ODGS	PixelSplat (P)	LatentSplat (P)	MVSplat (P)	PixelSplat (O)	MVSplat (O)	OmniSplat	OmniSplat+opt
Ballintoy	0, 35	0, 5, ..., 90	19.89 / 0.5674 / 0.4155	<b>21.78 / 0.7294 / 0.2729</b>	17.89 / 0.6572 / 0.3928	20.46 / 0.7433 / 0.2817	18.14 / 0.4102 / 0.5756	18.45 / 0.7034 / 0.3089	19.07 / 0.7751 / 0.3469	<b>21.46 / 0.8076 / 0.2580</b>
BeihaiPark	0, 55	0, 5, ..., 80	<b>21.38 / 0.6417 / 0.2837</b>	<b>20.37 / 0.6286 / 0.3051</b>	17.64 / 0.5379 / 0.3767	16.86 / 0.4977 / 0.4116	16.89 / 0.4015 / 0.5363	14.06 / 0.4564 / 0.4534	17.25 / 0.5324 / 0.3989	<b>17.62 / 0.5432 / 0.3733</b>
Cathedral	0, 50	0, 5, ..., 80	<b>19.54 / 0.5006 / 0.3809</b>	<b>17.08 / 0.5528 / 0.3270</b>	13.50 / 0.3863 / 0.4850	15.29 / 0.4623 / 0.4196	14.32 / 0.2504 / 0.6097	13.79 / 0.4555 / 0.4124	15.71 / 0.5288 / 0.4045	<b>16.24 / 0.5658 / 0.3672</b>
Coast	0, 45	0, 5, ..., 80	21.03 / 0.4943 / 0.4314	<b>22.53 / 0.7179 / 0.2839</b>	17.95 / 0.5629 / 0.4724	<b>21.74 / 0.5294</b> / 0.2828	17.78 / 0.3252 / 0.5968	18.02 / 0.6409 / 0.3138	19.89 / 0.6807 / 0.3580	<b>21.64 / 0.7368 / 0.2615</b>
Field	0, 45	0, 5, ..., 75	21.10 / 0.5530 / 0.4285	<b>25.70 / 0.7509 / 0.2636</b>	19.96 / 0.6498 / 0.4201	<b>25.54 / 0.7584</b> / 0.2970	19.61 / 0.3841 / 0.5985	20.04 / 0.6391 / 0.3745	22.20 / 0.6903 / 0.4038	<b>25.15 / 0.7116 / 0.2986</b>
Field	0, 50	0, 5, ..., 80	19.62 / 0.5883 / 0.3876	<b>20.03 / 0.6641 / 0.3096</b>	16.47 / 0.5805 / 0.4115	18.15 / 0.6152 / 0.3897	18.03 / 0.4017 / 0.5363	16.67 / 0.5549 / 0.4363	18.99 / 0.6267 / 0.3906	<b>19.68 / 0.6519 / 0.3415</b>
SecretGarden1	0, 40	0, 5, ..., 75	<b>20.91 / 0.6096 / 0.3470</b>	<b>19.57 / 0.6675 / 0.3021</b>	17.00 / 0.5812 / 0.4043	17.82 / 0.6030 / 0.3741	16.50 / 0.4073 / 0.5424	15.13 / 0.5545 / 0.4298	19.71 / 0.6814 / 0.3370	<b>20.71 / 0.7056 / 0.2926</b>
Shrines1	0, 45	0, 5, ..., 90	<b>18.34 / 0.4264 / 0.3979</b>	<b>16.88 / 0.4936 / 0.4174</b>	13.35 / 0.3260 / 0.5337	15.71 / 0.4179 / 0.5271	14.56 / 0.2643 / 0.5913	14.35 / 0.3434 / 0.4814	17.37 / 0.4712 / 0.4282	<b>17.37 / 0.4712 / 0.4282</b>
Temple3	0, 25	0, 5, ..., 70	<b>20.83 / 0.6062 / 0.3167</b>	<b>17.17 / 0.5869 / 0.3441</b>	12.41 / 0.4620 / 0.4762	13.63 / 0.4754 / 0.4555	13.02 / 0.3185 / 0.6215	12.30 / 0.4879 / 0.4152	16.24 / 0.6164 / 0.3657	<b>16.67 / 0.6513 / 0.3184</b>
Wulongting	0, 50	0, 5, ..., 95	<b>19.88 / 0.6722 / 0.3403</b>	<b>18.31 / 0.6938 / 0.2936</b>	15.01 / 0.6450 / 0.4135	16.04 / 0.6192 / 0.3652	15.56 / 0.3827 / 0.5816	16.10 / 0.6424 / 0.4236	19.13 / 0.7417 / 0.3253	<b>19.76 / 0.7633 / 0.2773</b>
average	-	-	<b>20.25 / 0.5660 / 0.3730</b>	<b>19.94 / 0.6486 / 0.3119</b>	16.30 / 0.5389 / 0.4386	18.12 / 0.5947 / 0.3804	16.44 / 0.3546 / 0.5810	15.89 / 0.5478 / 0.4049	18.50 / 0.6311 / 0.3794	<b>19.63 / 0.6608 / 0.3217</b>

Table D. Scene-wise quantitative results of 3D reconstruction on **OmniPhotos** dataset.

Scene	Ref. view	Test view	ODGS	PixelSplat (P)	LatentSplat (P)	MVSplat (P)	PixelSplat (O)	MVSplat (O)	OmniSplat	OmniSplat+opt
bar	6, 10	7, 8, 9	<b>17.59 / 0.5680 / 0.3151</b>	14.25 / 0.3583 / 0.4582	13.76 / 0.3802 / 0.5071	13.42 / 0.3278 / 0.5498	13.16 / 0.2092 / 0.6602	11.90 / 0.2472 / 0.5911	13.28 / 0.2862 / 0.5827	<b>16.90 / 0.6174 / 0.4315</b>
base	21, 25	22, 23, 24	<b>19.37 / 0.5790 / 0.3069</b>	16.04 / 0.4402 / 0.4162	14.03 / 0.4357 / 0.4664	15.79 / 0.4391 / 0.4723	13.48 / 0.1934 / 0.6492	12.42 / 0.3149 / 0.4942	15.41 / 0.4231 / 0.4593	<b>15.27 / 0.3996 / 0.4303</b>
cafe	41, 45	42, 43, 44	18.41 / <b>0.6789 / 0.3565</b>	16.95 / 0.4919 / 0.4498	15.52 / 0.4934 / 0.4787	17.17 / 0.4946 / 0.4764	15.05 / 0.2912 / 0.6352	13.28 / 0.4129 / 0.4828	18.73 / 0.6454 / 0.4220	<b>19.05 / 0.5758 / 0.3976</b>
canteen	74, 78	75, 76, 77	<b>16.42 / 0.4282 / 0.4944</b>	13.37 / 0.4187 / 0.5467	12.94 / 0.4511 / 0.5565	13.39 / 0.4141 / 0.5745	13.44 / 0.2678 / 0.6525	10.99 / 0.2637 / 0.6211	15.39 / <b>0.4578</b> / 0.5393	<b>15.16 / 0.4033 / 0.5318</b>
center	52, 56	53, 54, 55	<b>21.07 / 0.6161 / 0.3909</b>	17.17 / 0.5947 / 0.4146	16.70 / 0.6133 / 0.4874	19.01 / 0.5933 / 0.4656	16.07 / 0.3386 / 0.6366	11.95 / 0.4015 / 0.5175	20.48 / <b>0.6726</b> / 0.4130	<b>21.08 / 0.6652 / 0.3642</b>
center1	36, 40	37, 38, 39	19.37 / 0.6232 / 0.4377	16.33 / 0.6594 / 0.4464	16.12 / 0.6832 / 0.4784	16.35 / 0.6334 / 0.4868	15.31 / 0.2966 / 0.6798	12.10 / 0.3938 / 0.5798	20.59 / 0.7107 / 0.4459	<b>20.69 / 0.6956 / 0.4089</b>
corridor	10, 14	11, 12, 13	<b>21.10 / 0.6239 / 0.3130</b>	19.58 / <b>0.6934</b> / 0.3557	18.15 / 0.6235 / 0.4057	18.27 / 0.6533 / 0.4434	16.19 / 0.2591 / 0.6299	14.30 / 0.4323 / 0.4587	20.42 / 0.6104 / 0.3863	<b>20.56 / 0.6163 / 0.3969</b>
innovation	32, 36	33, 34, 34	<b>18.29 / 0.5288 / 0.3420</b>	14.						





Figure B. Qualitative comparison on OmniBlender dataset.



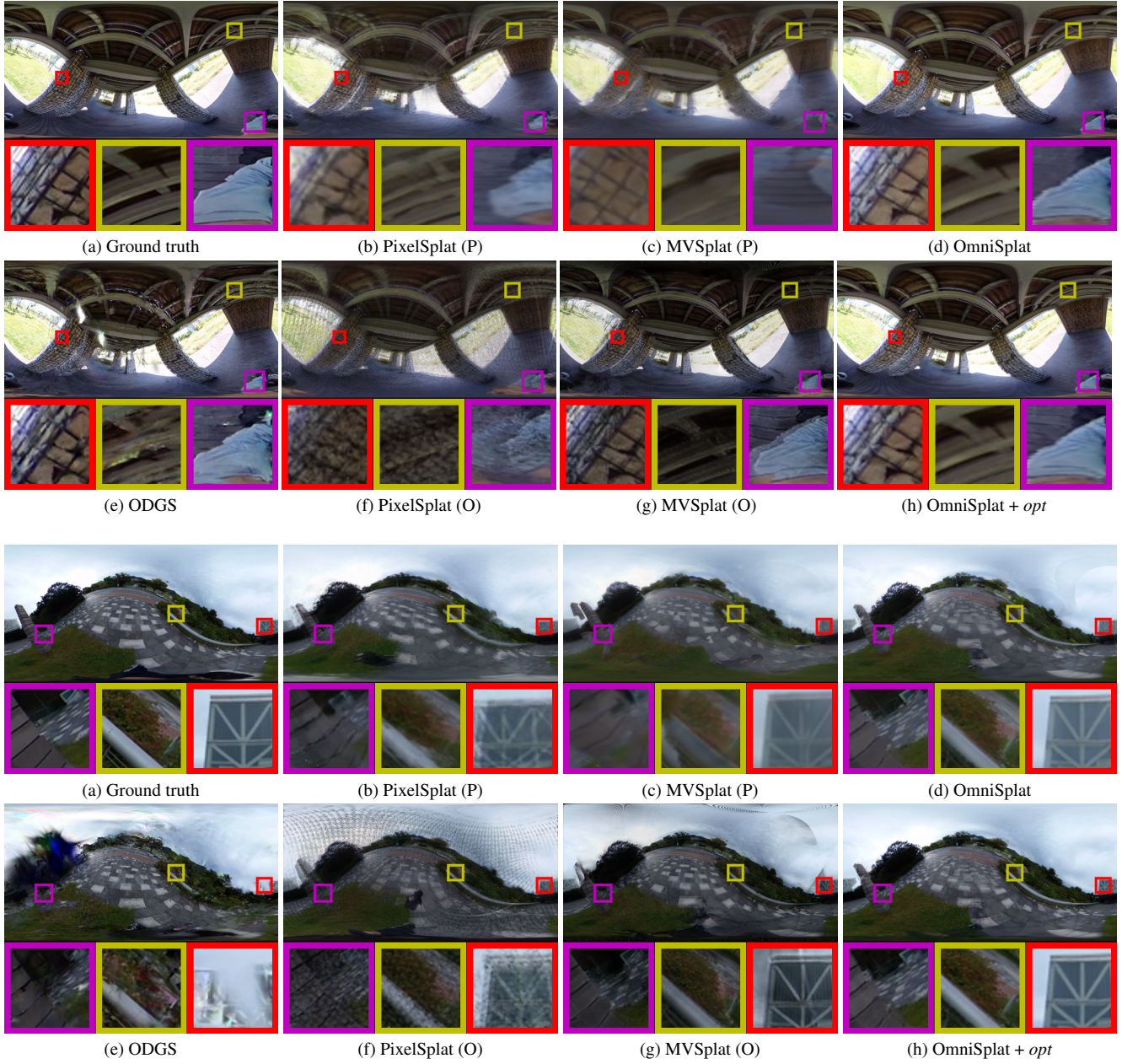


Figure C. Qualitative comparison on Ricoh dataset.



Figure D. Qualitative comparison on Ricoh dataset.



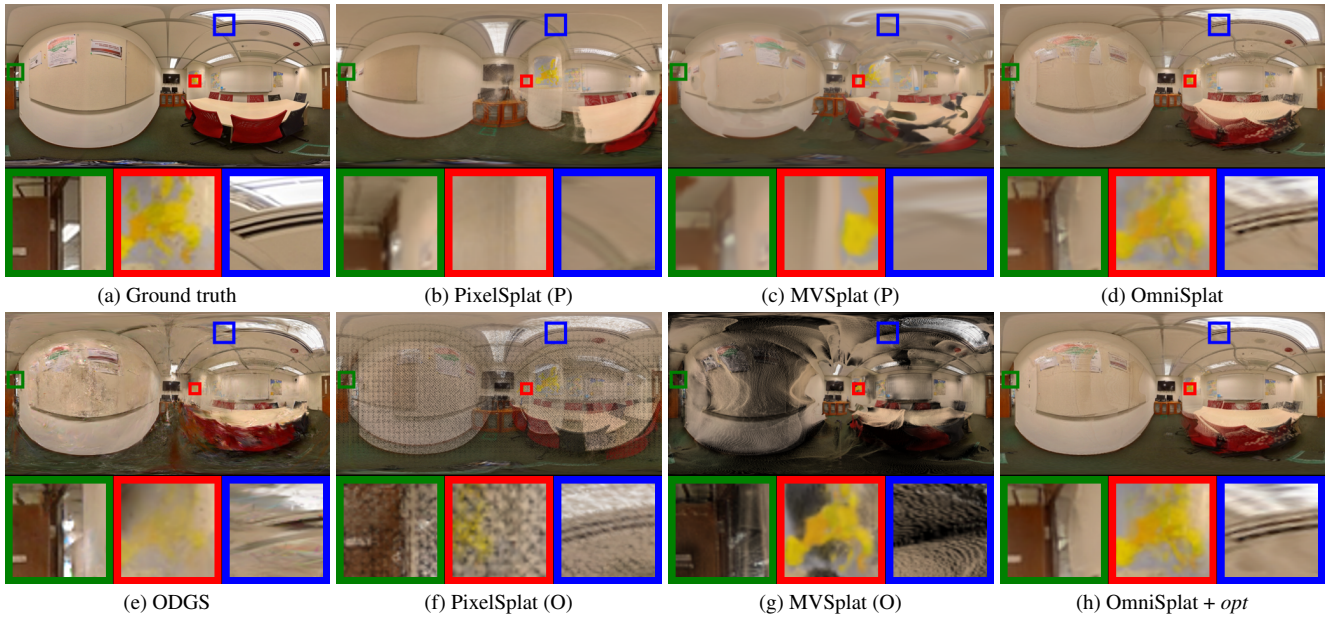


Figure E. Qualitative comparison on 360Roam dataset.

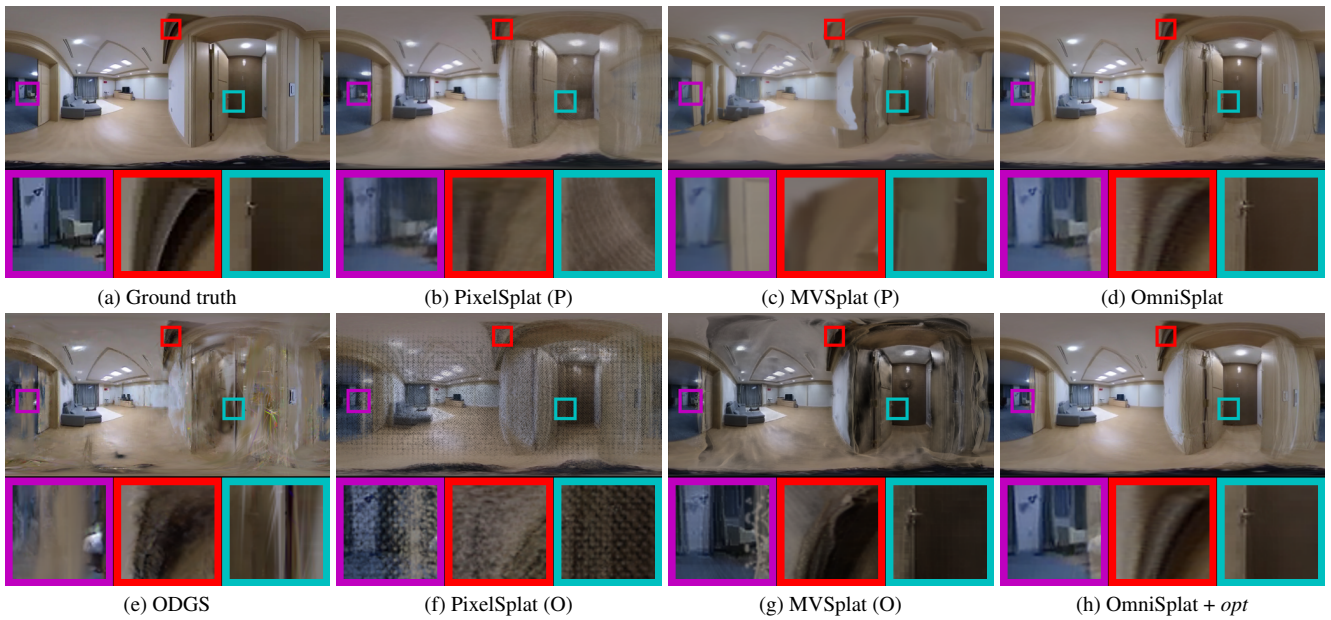


Figure F. Qualitative comparison on OmniScenes dataset.



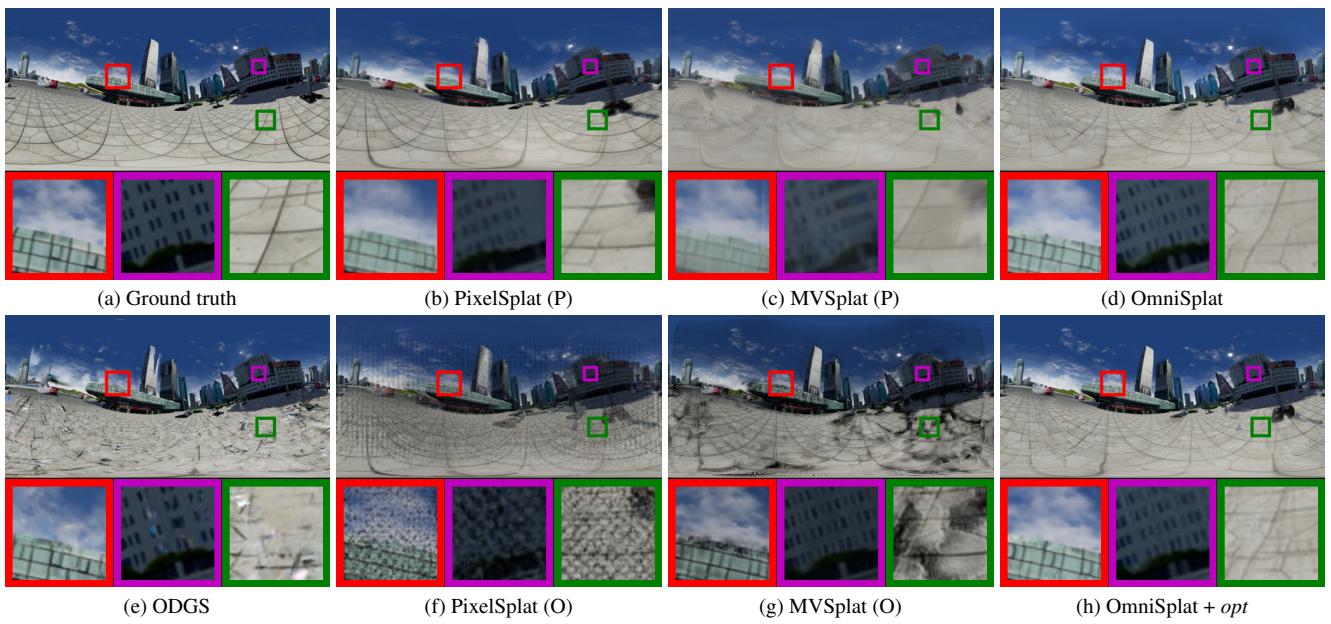


Figure G. Qualitative comparison on 360VO dataset.